JOURNAL OF VIROLOGY, Aug. 2010, p. 7625–7633 Vol. 84, No. 15
0022-538X/10/$12.00 doi:10.1128/JVI.00353-10

Structural Basis for the Inhibition of RNase H Activity of HIV-1 Reverse Transcriptase by RNase H Active Site-Directed Inhibitors[▽]

Hua-Poo Su,[1]* Youwei Yan,[1] G. Sridhar Prasad,[1] Robert F. Smith,[1] Christopher L. Daniels,[1] Pravien D. Abeywickrema,[1] John C. Reid,[1] H. Marie Loughran,[2] Maria Kornienko,[1] Sujata Sharma,[1] Jay A. Grobler,[3] Bei Xu,[1] Vinod Sardana,[1] Timothy J. Allison,[1] Peter D. Williams,[2] Paul L. Darke,[1] Daria J. Hazuda,[3] and Sanjeev Munshi[1]

Departments of Global Structural Biology,[1] Medicinal Chemistry,[2] and Antiviral Research,[3] Merck Research Laboratories, P.O. Box 4, West Point, Pennsylvania 19486

Received 16 February 2010/Accepted 11 May 2010

HIV/AIDS continues to be a menace to public health. Several drugs currently on the market have successfully improved the ability to manage the viral burden in infected patients. However, new drugs are needed to combat the rapid emergence of mutated forms of the virus that are resistant to existing therapies. Currently, approved drugs target three of the four major enzyme activities encoded by the virus that are critical to the HIV life cycle. Although a number of inhibitors of HIV RNase H activity have been reported, few inhibit by directly engaging the RNase H active site. Here, we describe structures of naphthyridinone-containing inhibitors bound to the RNase H active site. This class of compounds binds to the active site via two metal ions that are coordinated by catalytic site residues, D443, E478, D498, and D549. The directionality of the naphthyridinone pharmacophore is restricted by the ordering of D549 and H539 in the RNase H domain. In addition, one of the naphthyridinone-based compounds was found to bind at a second site close to the polymerase active site and non-nucleoside/nucleotide inhibitor sites in a metal-independent manner. Further characterization, using fluorescence-based thermal denaturation and a crystal structure of the isolated RNase H domain reveals that this compound can also bind the RNase H site and retains the metal-dependent binding mode of this class of molecules. These structures provide a means for structurally guided design of novel RNase H inhibitors.

In 2007, approximately 30 million people worldwide were infected with HIV, with an additional 2.5 million newly infected individuals (36). At present, there are 24 antiretroviral inhibitors that have been approved by the U.S. Food and Drug Administration (FDA) (9). These have been used for the treatment of HIV infections in combination therapy by simultaneously targeting multiple viral mechanisms. Despite the achievements of the highly active antiretroviral therapy (HAART), the rapid emergence of viral resistance to therapies remains a challenge.

Currently, all but two of the FDA-approved antiretroviral drugs target the function of the three virus-encoded enzymes: protease, integrase, and reverse transcriptase (RT); the other two block fusion and/or entry of the virus (9). For RT, there are two classes of inhibitors that affect the polymerase function, the nucleoside and non-nucleoside reverse transcriptase inhibitors (NRTIs and NNRTIs, respectively). HIV RT, a heterodimer consisting of 66- and 51-kDa subunits, acts as a DNA polymerase and plays a central role in the viral life cycle (11). Concomitant to the polymerase function, RT has RNase H activity that is unique to the C terminus of the p66 subunit. This activity is required for processing the tRNA primer used to begin minus-strand DNA synthesis and degradation of the viral RNA during synthesis, followed by preparation of the polypurine tract DNA-RNA hybrid, which serves as the primer for positive-strand DNA synthesis (11, 34). Mutations in the RNase H domain have demonstrated that RNase H activity is critical for the survival of the virus (4, 17, 25). Essential for RNase H activity is a group of three carboxylate-containing amino acid residues, conserved in the class of polynucleotidyl transferases and a fourth conserved in RNase H (38).

For decades, despite the knowledge of a role for RNase H activity in the HIV infection process (12, 13), the development of RNase H-specific inhibitors has been confounded by the interdependence between polymerase and RNase H activities. Compounds that are either nucleoside or non-nucleoside inhibitors have been reported to inhibit both the polymerase and RNase H activities (1, 35); however, the mechanism(s) of RNase H inhibition are poorly understood. A recent crystal structure of a compound which displayed RNase H inhibition, DHBNH, revealed a binding site adjacent to the NNRTI binding site and polymerase catalytic site (16). This site is located ~50 Å from the active site of the RNase H domain. During the preparation of the present study, two reports were published with inhibitors bound to the RNase H active site (15, 18).

The structures presented here show compounds that bind directly to the RNase H active site of HIV RT. Compounds containing the metal-binding naphthyridine pharmacophore have previously been shown to inhibit HIV integrase in a manner that involves coordinating divalent ions at the active site (14). Although the coordination of metal ions has successfully been exploited in the design of HIV integrase inhibitors,

* Corresponding author. Mailing address: 770 Sumneytown Pike, P.O. Box 4, WP14-1101, West Point, PA 19486. Phone: (215) 652-7347. Fax: (215) 652-6345. E-mail: hua-poo_su@merck.com.

▽ Published ahead of print on 19 May 2010.

TABLE 1. Parameters for compound crystals MK1 RT (3LP0), MK2 RT (3LP1), MK3 RT (3LP2), and MK3 RNase H (3LP3)

Parameter	Compound crystal PDB ID[a]			
	MK1 RT (3LP0)	MK2 RT (3LP1)	MK3 RT (3LP2)	MK3 RNase H (3LP3)
Resolution (Å)	50–2.80	50–2.23	50–2.80	50–2.80
Completeness (%)	91.8 (83.4)	96.3 (97.2)	97.1 (98.4)	100 (100)
Avg redundancy (%)	3.6 (2.5)	5.1 (4.8)	5.1 (5.1)	5.8 (5.7)
R_{sym} (%)	4.3 (43.0)	4.9 (25.1)	5.8 (39.0)	9.8 (36.9)
$<I/\sigma I>$	23.4 (2.3)	26.1 (4.9)	27.0 (4.4)	20.2 (6.7)
Space group	$C222_1$	$C222_1$	$C222_1$	$P3_1$
a (Å)	118.3	118.8	117.5	51.3
b (Å)	154.2	155.3	154.8	51.3
c (Å)	153.2	155.2	155.8	112.8
α (°)	90	90	90	90
β (°)	90	90	90	90
γ (°)	90	90	90	120
RMS deviations				
Bond length (Å)	0.007	0.006	0.007	0.006
Bond angle (°)	1.046	0.962	1.028	1.029
No. of nonhydrogen atoms used in refinement	7,918	8,035	7,914	2,104
No. of water atoms	52	175	62	18
No. reflections total/no. reflections free set	30,644/1,618	64,255/3,410	32,509/1,728	7,751/387
R_{work}/R_{free} (%)	24.8/31.0	26.8/29.2	24.9/29.6	22.9/28.8

[a] Values in parentheses are for the highest-resolution bin.

a detailed understanding of the metal coordination and inhibitor binding remain elusive. The structures reported here demonstrate that the inhibitors bind RNase H by coordinating two metal ions, engaging the conserved DDE motif of the active site. This is consistent with the two-metal ion mechanism proposed based on structures of HIV RNase H (7) and other bacterial RNases H (27–29, 37). In addition, since naphthyridinones are capable of coordinating two metal ions simultaneously, there could be two possible orientations for binding, depending on which metal ion is coordinated by each site. No energetic preference was observed for the two binding orientations in molecular modeling studies (14). However, the structures reported here describe a single orientation for binding, determined by specific interactions with the protein. This understanding could be critical in structure-guided design of HIV RNase H-specific inhibitors that may offer a new opportunity to treat patients resistant to currently available regimens of antiretroviral therapies.

RNases H play a critical role in almost all organisms (2). There are two types of RNases H found in humans. HIV RNase H is similar to RNase H1, which is likely to be critical in humans as the *Rnaseh1*$^{-/-}$ mice arrest during development with defects in mitochondrial DNA replication (3). In addition, in humans, mutations in type II RNase H have been associated with the neurological disorder, Aicardi-Goutieres syndrome (5). Therefore, the development of inhibitors specific to HIV RNase H is critical in order to avoid potential adverse effects.

MATERIALS AND METHODS

Cloning, expression, and purification. (i) Full-length RT. The sequence of the p66 subunit of HIV RT (strain HxB2) was cloned for bacterial expression under a T7 promoter, as previously described (23). The full-length protein contains a lysine-to-arginine (K103N) mutation. Plasmids were transformed into BL21(DE3) cells and grown to an optical density of 0.8 at 600 nm before induction with 1 mM IPTG (isopropyl-β-D-thiogalactopyranoside). After 4 h of induction, cells were pelleted by centrifugation. Cell pellets were resuspended in lysis buffer containing 50 mM Tris-HCl (pH 7.8), 4 mM EDTA, 5% glycerol, 60 mM NaCl, 2 mM dithiothreitol (DTT), 2 mM $MgCl_2$, 10 μg of DNase I/ml, and one protease inhibitor cocktail tablet (Roche, Basel, Switzerland) per 50 ml of lysis buffer. Cells were further lysed by using a microfluidizer. Protein was purified on DE-52, followed by affinity purification on a heparin column that separates p66/p51 heterodimers from p66 homodimers. Fractions containing the p66/p51 heterodimer were subject to purification using a MonoS column, followed by gel filtration. The protein was concentrated to 30 to 50 mg/ml in buffer containing 20 mM Tris-HCl (pH 8.0), 150 mM NaCl, and 2 mM DTT.

(ii) RNase H domain of RT. A gene was synthesized (DNA 2.0, Burlingame, CA) that encodes a thrombin-cleavable His_6 tag, followed by residues 427 to 562 of RT, based on the sequence used by Davies et al. (7). Bacterial expression was carried out as described above for the full-length RT. Cell pellets were resuspended in a buffer containing 20 mM HEPES (pH 7.2), 10 mM $MgCl_2$, 2 mM DTT, 50 mM NaCl, 25 μg of Benzonase/ml, 15,000 U of lysozyme/ml, and one tablet of Complete EDTA-free protease inhibitor (Thermo Scientific, Rockford, IL) per 50 ml of lysis buffer. Cells were lysed by Dounce homogenization and microfluidization. Protein was purified on a nickel-NTA column by using an imidazole gradient for elution. The protein was concentrated and dialyzed overnight against a buffer containing 20 mM HEPES (pH 7.5) and 50 mM NaCl. The His_6 tag was removed by proteolysis with thrombin. Residual, tagged protein was removed by binding to a nickel-NTA column and untagged protein was further purified by gel filtration. RNase H was buffer exchanged against 20 mM potassium phosphate (pH 7.0) and concentrated to 8 to 10 mg/ml.

ThermoFluor. Fluorescence-based thermal stability assay experiments were carried out on 384-well plates in quadruplicates in a buffer containing 20 mM HEPES (pH 7.5), 100 mM NaCl, 0.5 mM EDTA, and 50 μM the fluorescent dye, 1-anilinonaphthalene-8-sulfonic acid (ANS; Invitrogen, Carlsbad, CA) (6, 31). RT was used at a concentration of 16 μM. $MgCl_2$ or $MnCl_2$ was added at a final concentration of 5 mM, and inhibitors were added at 50 μM. Each 4-μl sample was overlaid with 1 μl of silicone oil by centrifugation. The temperature was scanned from 25 to 90°C in 1° increments. The data were analyzed by using ThermoFluor v1.3.7 software.

Crystallization. To obtain crystals of full-length RT, the NNRTI, nevirapine (24), was added to the protein at a final concentration of 1 mM prior to crystallization. Full-length RT, complexed with nevirapine, was crystallized in sitting drops using a 1:1 mixture of protein and reservoir buffer containing 100 mM sodium cacodylate (pH 6.8) and 800 mM sodium citrate. Larger crystals were obtained by macroseeding and continued to grow for a month after seeding. For inhibitor soaks, crystals were harvested into reservoir solution with addition of 50 mM $MnCl_2$ and 1 mM inhibitor. The inhibitors were added from a stock solution solubilized in dimethyl sulfoxide (DMSO). Crystals of full-length RT were grown and soaked with inhibitor at room temperature. Before data collection, crystals

TABLE 2. *In vitro* and antiviral IC_{50}s, cell cytotoxicity concentrations, and structures of MK1, MK2, and MK3[a]

Compound	*In vitro* IC_{50} (μM)	Antiviral IC_{50} (μM)	Cell cytotoxicity concn (μM)	Structure
MK1	0.11	2.8	>50	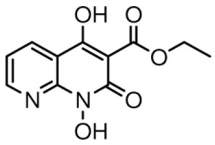
MK2	0.12	3.0	39	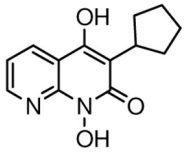
MK3	0.22	9.0	>50	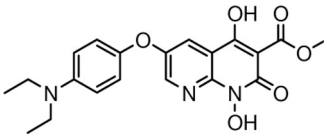

[a] IC_{50}, 50% inhibitory concentration.

were transferred into a buffer containing the reservoir solution with the addition of 25% glycerol and vitrified by submersion into liquid nitrogen.

The isolated RNase H domain was crystallized in a buffer containing 100 mM sodium citrate (pH 5.0) and 15 to 20% PEG-8000. Crystals were harvested for inhibitor soaks in the reservoir solution with the addition of 50 mM $MnCl_2$ and 1 mM inhibitor. Crystals of the isolated RNase H domain were grown and soaked with inhibitor at 4°C. Manipulation of crystals for cryoprotection was performed at room temperature. It was found that $MgCl_2$ could be used, but inhibitors did not appear in density consistently. When the inhibitor was present, there was no difference between the mode of binding with Mg^{2+} or Mn^{2+}. For data collection, crystals were transferred into a buffer containing the reservoir solution with addition of 25% glycerol and vitrified by direct exposure to a cryocooled nitrogen gas stream.

Data from the full-length RT crystals were collected on the IMCA-CAT beamline at the Advanced Photon Source/Argonne National Labs. The data from the RNase H crystals were collected on a Rigaku FR-E generator using a Saturn 944+ detector. All data were processed and scaled by using HKL2000 (30). Phases were obtained by rigid body refinement using Refmac5 (26). For full-length RT, a reference structure that is similar to published structures from the group (PDB code: 2RF2) (39) was used as a starting model for phasing. The structure of the RNase H domain (PDB code: 1HRH) (7) was used to phase the RNase H:MK3 structure directly by rigid-body refinement. Models were built by iterative cycles of rebuilding with MIFit and Coot (10) and refinement with Refmac5 (26). Model geometries were verified with Procheck (21). Images of the structures were rendered with PyMOL (8).

RNase H activity assay. RNase H activity of full-length HIV RT was measured using a substrate generated by annealing the RNA with the sequence 5′-CCCC CUCUCAAAAACAGGAGCAGAAAGACAAG to a DNA oligonucleotide 5′-biotin-GTCTTTCTGCTC. Reactions were carried out with 2.0 nM RT, inhibitor, and RNA/DNA hybrid duplex substrate (13 nM) in a solution containing 50 mM Tris-HCl (pH 7.8), 80 mM KCl, 6 mM $MgCl_2$, 1 mM DTT, 0.1 mM EGTA, 0.2% PEG-8000, and 1 to 10% DMSO. Reactions were incubated at 37°C for 60 min and then quenched by the addition of EDTA. RNA strand cleavage results in the dissociation of the 5′-biotinylated DNA strand, which is then annealed to a ruthenium-labeled, cDNA oligonucleotide, 5′-ruthenium-GAGCAGAAA GAC. The resulting double-stranded duplex DNA product is quantitated in an ECL screen format using Dynabeads M-280 coated with streptavidin (BioVeris Corp., Gaithersburg, MD) and read on a BioVeris M384 analyzer.

Protein data bank accession numbers. PDB files and structure factors have been deposited into the Protein Data Bank with the following PDB IDs: 3LP0 for MK1 with full-length RT, 3LP1 for MK2 with full-length RT, 3LP2 for MK3 with full-length RT, and 3LP3 for MK3 with the RNase H domain.

RESULTS

Compounds binding to RNase H active site. Crystallization conditions were screened to find a reproducible, robust crystal form into which small molecule inhibitors could be stably soaked. In screens using the HxB2 strain of RT, crystals were obtained in buffer containing sodium cacodylate with sodium citrate. This condition requires cocrystallization with an NNRTI, such as nevirapine (19). Although the crystallization condition is different, the crystal form is the same as one that has been previously described (22). We have used these crystals to soak inhibitors for many weeks without significant impact on diffraction quality (Table 1).

Crystals of full-length RT were used to provide a structural basis for the inhibition of RNase H activity for a series of naphthyridinone-based compounds. This series of inhibitors was designed to bind the metal ions required for polymerase and RNase activity of RT. Based on previous studies on the compounds that inhibit HIV integrase, it was thought that these compounds may bind to metal ions and directly interact with the RNase H active site of RT (14). The compounds were tested for their ability to inhibit RNase H activity in an assay using full-length RT and a RNA-DNA duplex substrate, in the presence of Mg^{2+} (Table 2) (P. D. Williams et al., unpublished data). To understand their mechanism of action, the inhibitors were soaked into crystals in the presence of 50 mM Mn^{2+}. Mn^{2+} was used as a surrogate for Mg^{2+} since soaking experiments with Mg^{2+} could not reproducibly yield structures with inhibitor bound. Crystals soaked with compound MK1 diffracted to 2.8 Å (Table 1). The electron density revealed direct binding of MK1 to the RNase H active site. This site is ~50 Å from the NNRTI site, which is occupied by the cocrystallized nevirapine (Fig. 1A). There is no density to support MK1 binding to the polymerase site. There are interactions between MK1 (Fig. 1B) and two Mn^{2+} ions, which are coordinated by the RNase H active site residues D443, E478, D498, and D549

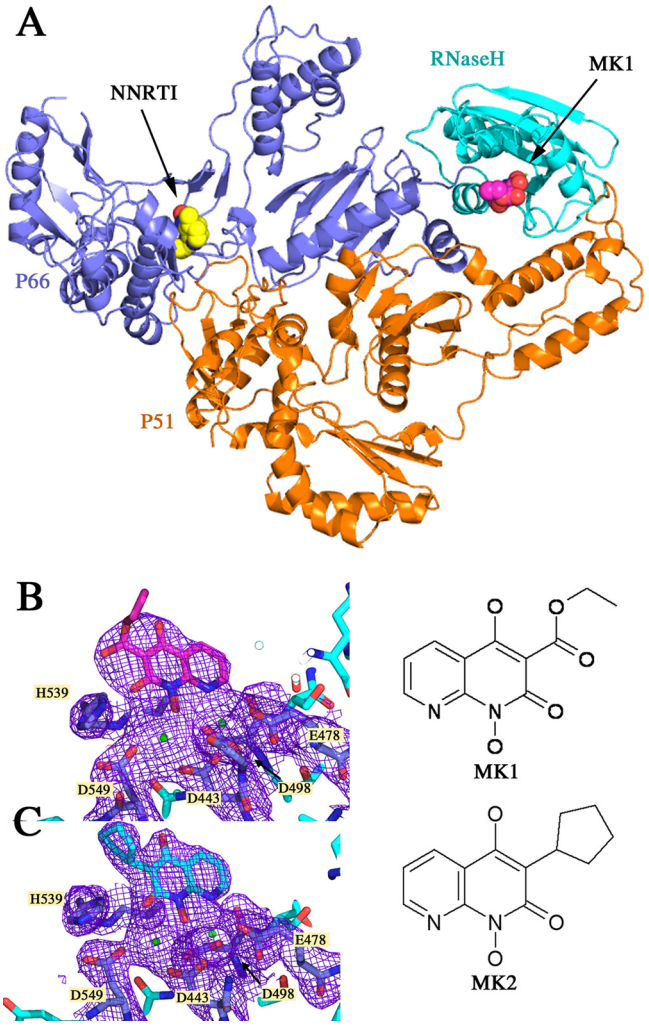

FIG. 1. Structures of compounds MK1 and MK2 bound to the RNase H active site of HIV-1 RT. (A) The structure of RT is shown as a ribbon diagram, with the p66 subunit colored blue and the RNase H domain colored a lighter shade. The p51 subunit is colored orange. The inhibitor, MK1, is shown as a space-filling model in magenta, bound to the RNase H active site. On the opposite side of RT is the NNRTI pocket, which contains the NNRTI, nevirapine (yellow), required for crystallizing RT. (B) MK1 is shown on the left, bound to the RNase H active site. The electron density (sigmaA weighted 2Fo-Fc map [33] contoured at 1σ) is shown in purple. The naphthyridine rings of the compound coordinate two Mn^{2+} ions (green) with the catalytic site residues. (C) The structure of the inhibitor, MK2 (cyan), binds to the active site in a similar pose to MK1. The electron density (sigmaA weighted 2Fo-Fc map contoured at 1σ) is shown in purple and a two-dimensional image of the inhibitor is shown on the right.

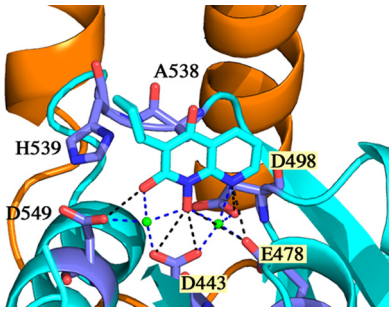

FIG. 2. Binding of MK2 to the RNase H active site of RT. Close-up view of MK2 (cyan) bound to the active site. The two Mn^{2+} ions are shown in green, and bonds to the Mn^{2+} ions are shown in blue. One Mn^{2+} is coordinated by carbonyl oxygens from D443 and D549 and two oxygens of the naphthyridinone. The other Mn^{2+} is coordinated by the other carbonyl oxygen of D443, E478, D498, and the naphthyridine moiety of the compound. In addition to contacts with the metal ions, the inhibitor also interacts with a loop in RT containing A538 and H539. Select protein 1:1 inhibitor bonds are shown in black.

(Fig. 1B). In addition, G444, S499, A538, H539, V552, and S553 contribute to the binding site. The electron density is not well resolved for the ethyl group of the compound (Fig. 1B).

One crystal was found that permitted the collection of a 2.2-Å data set with the compound, MK2. The structure of MK2 shows similar coordination of two Mn^{2+} ions with the active site as observed with MK1. MK2, like MK1, binds to the RNase H active site, and there is no density supporting interaction with the polymerase site. The binding pocket for MK2 is made up of the same residues as those for MK1, which is not unexpected since the two compounds differ only slightly with the ethyl formate of MK1 replaced by cyclopentane in MK2. In the structure of MK2, there is well-resolved electron density for the entire compound (Fig. 1C).

Metal ion coordination. The naphthyridinone core of MK1 and MK2 binds to the RNase H active site in a single orientation. The 1-hydroxyl group coordinates both metal ions, with each ion being additionally coordinated by either the oxygen or the other naphthyridine nitrogen. It was originally proposed that the naphthyridinones could bind in two orientations relative to the axis of the central hydroxyl group (14); however, in the structures of MK1 and MK2, only one binding orientation of the naphthyridinone was observed. One Mn^{2+} ion is coordinated by D443, E478, and D498 of the active site and the central hydroxyl group and flanking nitrogen of the inhibitor. The other Mn^{2+} is coordinated by D443 and D549 and the central hydroxyl group and flanking oxygen of the inhibitor (Fig. 2). D549 is located on the C-terminal helix and is usually not resolved or poorly ordered in other crystal structures (32). Previous nuclear magnetic resonance studies have indicated that coordination of the second Mn^{2+} may order D549 (32). In the structure of MK1, H539 also appears to be ordered. The Nε of H539 is within hydrogen bonding distance (2.7 Å) to the naphthyridinone oxygen. In an alternate rotamer, the H539 Nε is 3.2 and 3.3 Å from the two carboxylate oxygens of D549, and the Nδ is 3.0 Å from the carboxylate oxygen of the inhibitor. In the structure of RT complexed to MK2, the inhibitor appears shifted away from H539, which primarily appears to be stabilized by a 2.7-Å hydrogen bond to one of the D549 carboxylate oxygens. In both structures, the position of H539 sterically prohibits the naphthyridinone from flipping and binding in the opposite orientation relative to the central hydroxyl-metal coordination, defining the unidirectional binding.

Inhibitor binding near the NNRTI/polymerase site. One of the inhibitors synthesized during the lead optimization process appears to bind at a different site, despite containing the metal-binding, naphthyridinone core. When the structure of a third compound (MK3) was determined, the electron density indicated that the inhibitor bound to a site close to the NNRTI

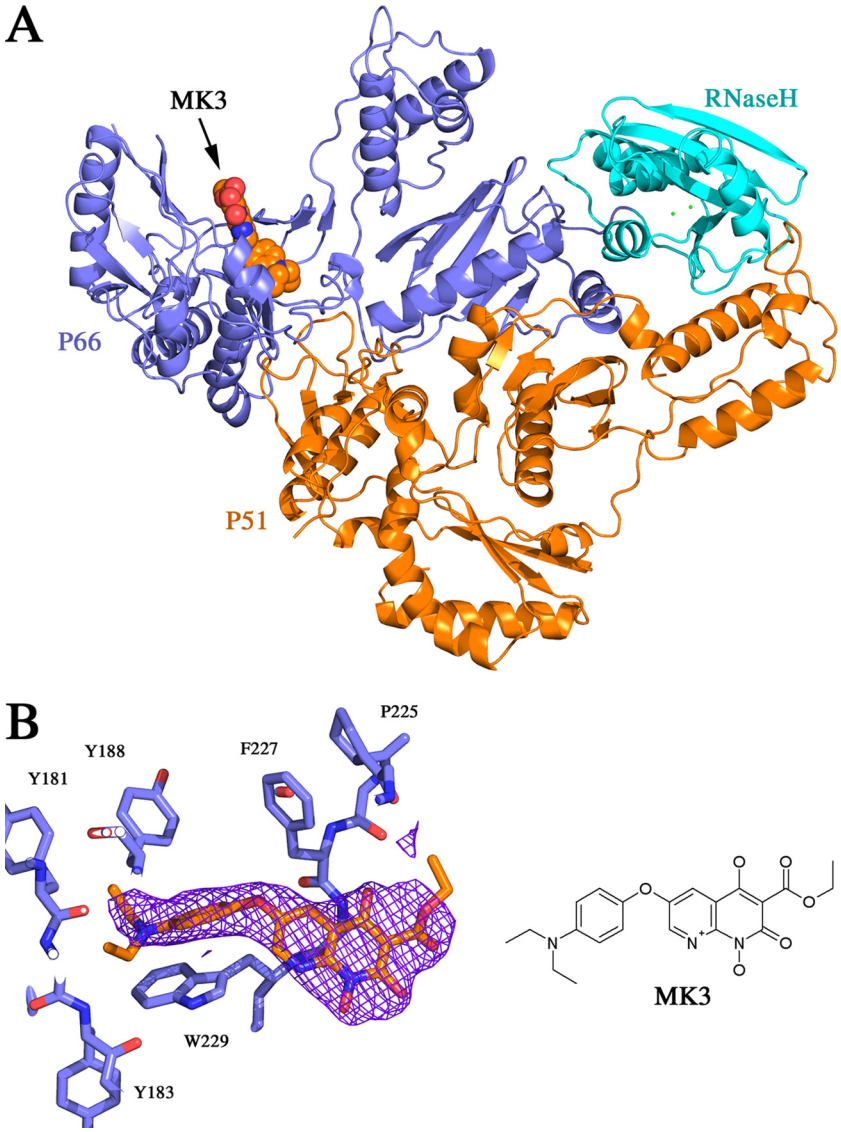

FIG. 3. Binding of MK3 to a site close to the NNRTI site. (A) The full-length RT is shown as ribbons and colored with the p66 subunit in blue and the p51 subunit in orange. Two Mn^{2+} ions (green) are present in the active site of the RNase H domain (green). The inhibitor, MK3 (orange), is shown as a space-filling model binding away from the RNase H domain. The binding of MK3 displaces the nevirapine used for cocrystallization. (B) The interactions of MK3 are mostly made by hydrophobic interactions and are metal independent. The electron density is shown in dark blue (sigmaA weighted 2Fo-Fc map contoured at 1σ).

pocket, distant from the RNase H site (Fig. 3A), and there was no density for the inhibitor at the RNase H site. The density at the new site indicated that the interactions with the protein were not mediated by metal coordination. Led by the diethylaminophenoxy group, the inhibitor is inserted into a relatively hydrophobic pocket lined by numerous residues, which include L100, V108, Y181, Y183, D186, L187, K223, F227, L228, W229, and L234. The pocket is adjacent to the NNRTI pocket, with a slight overlap which is sufficient to displace the cocrystallized nevirapine. Superposition of the structures showed that the ethylamine of MK3 overlaps with the nevirapine present in the MK1 and MK2 structures. This finding might suggest that the naphthyridinone core-containing compounds bind to RT at more than one site and yet may specifically inhibit the RNase H activity of RT. Although the naphthyridinone makes some interactions at the opening of the hydrophobic pocket, the hydrophobic interactions are largely mediated by the diethylaminophenol substituent that is unique to MK3.

Metal dependence of compound binding. To further probe the metal dependence for compound binding to RT, the addition of metals and inhibitors were tested for their ability to stabilize protein against thermal denaturation (31). ThermoFluor-based measurements of thermal stability indicate a small increase in protein stability, manifesting a 1 to 1.5°C shift in melting temperature when either Mg^{2+} or Mn^{2+} is added (Fig. 4). However, when compounds are added in the presence of either ion, there is a significantly larger shift in melting temperature (ca. 3 to 4°C). In the absence of metal, the shift is small and within the error of the experiment of unliganded protein. MK3 binding, like MK1 and MK2 binding, also ap-

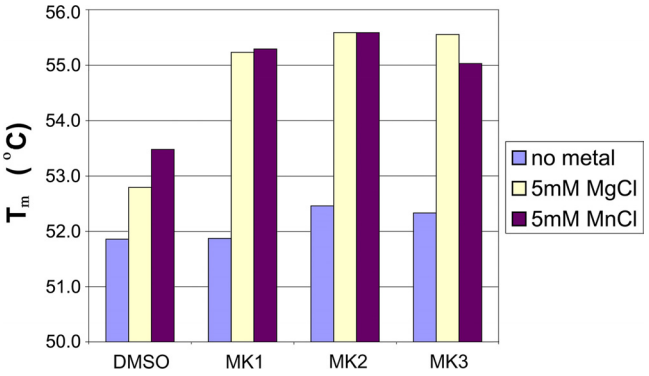

FIG. 4. ThermoFluor analysis of metal dependence on inhibitor binding to full-length RT. Fluorescence-based thermal denaturation temperatures for RT in the absence (DMSO control) or presence of inhibitor. Experiments are conducted in the absence of metal (blue), the presence of Mg^{2+} (yellow), or the presence of Mn^{2+} (purple). There is a metal-dependent increase in thermal stability for all three inhibitors.

pears to be metal dependent, suggesting that an additional metal-dependent binding site may be present, possibly binding the RNase H active site similar to MK1 and MK2.

MK3 binding to the RNase H site. Since MK3 appeared to have a metal-dependent mechanism of binding, we proposed that the size of the compound prohibited its binding to the RNase H site due to constraints of the crystal packing with full-length RT. In the $C222_1$ space group of the full-length RT crystals, the RNase H domain is packed closely with the RNase H domain of a neighboring molecule in the crystal lattice, with an ~20-Å distance between the active sites and a small channel that could allow small inhibitors to diffuse through. Empirically, it appears that small compounds could be soaked into the crystal; however, relatively larger compounds failed to bind. In order to address this possibility, the isolated RNase H domain was used to access a different crystal packing that would accommodate larger compounds. Crystals of the RNase H domain were soaked with MK3 in the presence of Mn^{2+}. As shown in Fig. 5A, MK3 binds directly to the active site of the isolated RNase H domain. The inhibitor appears to bind and

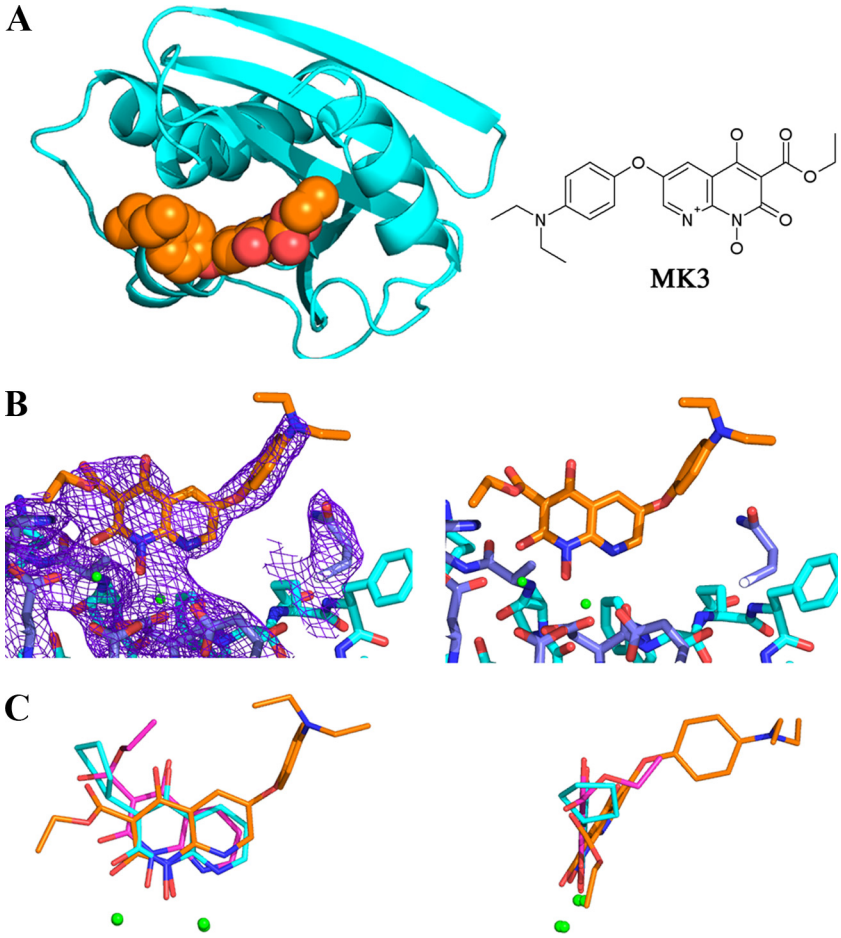

FIG. 5. The structure of MK3 bound to the active site of the isolated RNase H domain of RT. (A) MK3 is shown in orange as a space-filling model bound to the active site of RNase H (ribbons). For reference, the two-dimensional representation for the inhibitor is shown on the right. (B) The electron density map (sigmaA weighted 2Fo-Fc map contoured at 1σ) for MK3 bound to RNase H is shown in purple on the left. Binding without the electron density map is shown on the right. The Mn^{2+} ions are shown in green. (C) MK3 from the RNase H domain crystals is overlaid on top of the inhibitors MK1 and MK2 from the full-length RT crystals based on structural alignment of the RNase H domain. The two Mn^{2+} ions, which bind each inhibitor, do not move significantly. The metal-coordinating naphthyridine of MK3 is rotated (left) and tilted out of the plane of MK1 and MK2 (right) due to interactions mediated by the additional benzyl ring.

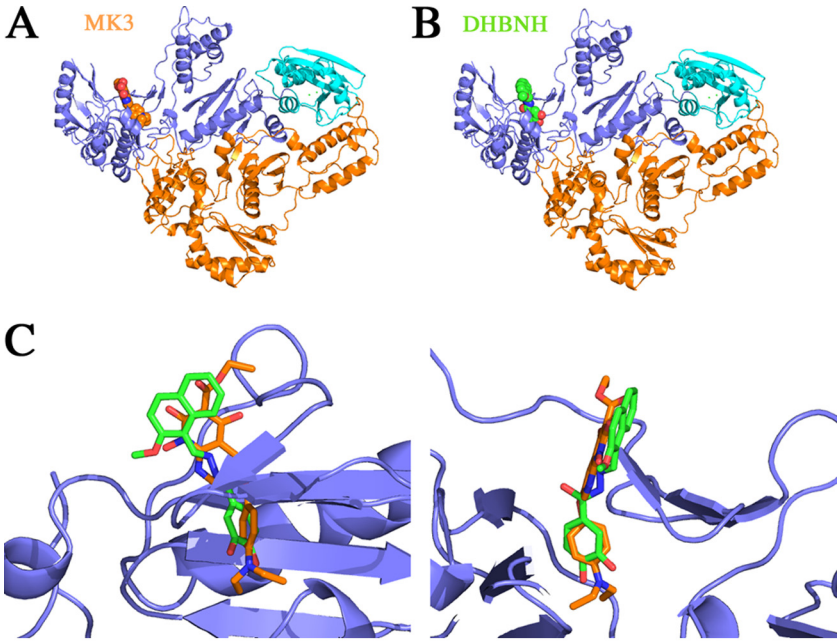

FIG. 6. Comparison of the binding of MK3 and DHBNH away from the RNase H active site. (A) The structure of full-length RT is shown as a ribbon diagram (p66 subunit in blue and p51 subunit in orange) bound to MK3 (orange) on the left and DHBNH (green) on the right(16). (B) The two inhibitors are overlaid with MK3 in orange and DHBNH in green, showing a common binding site for both inhibitors. A rotated perspective of the binding site is shown on the right.

coordinate metal ions in the same way as MK1 and MK2 binding to full-length RT (Fig. 5B). Although the RNase H domain crystal accommodates soaking of MK3, there is still a neighboring molecule close to the inhibitor in this crystal form. As a result, the phenyl ring of MK3 appears to pack against Q500 of the neighboring molecule. This causes a slight shift in the plane of the MK3 naphthyridinone, relative to its binding in the other two compounds (Fig. 5C). This may indicate that there is some range of acceptable conformations for the metal-coordinating pharmacophore, which may benefit from additional development beyond the central naphthyridinone. Although metal coordination is the central feature of binding, there is room to accommodate a variety of groups appended to the naphthyridine core to develop the structure-activity relationship and improve compound potency and specificity.

DISCUSSION

The structures presented here represent inhibitors bound to the active site of RNase H, which provide a basis for further development of compounds that could specifically inhibit this critical function of reverse transcriptase. Many of the interactions found in the structures are mediated by metal coordination, and further development of the structure-activity relationships, with consideration of direct interactions with the protein, may provide better potency and specificity for the inhibition of HIV-1 RNase H activity. All of the inhibitors share a naphthyridinone core that coordinates two metal ions with the conserved acidic, active site residues D443, E478, D498, and D549. In addition, the naphthyridinone is sandwiched by a loop containing residues A538 and H539 on one side and N474 on the opposite side. Sequence comparison with human RNase H shows that N474 and H539 are conserved. The A538 is a Gly in human RNase H1.

Even though the compounds were initially found to inhibit RNase H activity in the presence of Mg^{2+} *in vitro*, the structures were obtained by soaking inhibitors in the presence of Mn^{2+}. Soaking in the presence of Mg^{2+} was also tested, but inhibitors did not reliably bind with enough occupancy to provide well-resolved electron density. Frequently, only one of the two Mg^{2+} sites were occupied if inhibitor was not present, but if the compound was present in the structure, it binds and coordinates the metal ions similarly for both Mn^{2+} and Mg^{2+} (data not shown).

Using crystals of full-length reverse transcriptase, the inhibitor MK3 appears to bind to an alternative site that is close to the polymerase active site and adjacent to the NNRTI binding site. However, further experiments showed that the inhibitor binds to the protein in a metal-dependent manner, suggesting that it binds to the RNase H active site. Unlike the binding to the RNase H active site, binding to the alternate site appears to be predominantly mediated via the hydrophobic interactions with the diethylaminophenoxy group unique to MK3. It is difficult to reconcile whether the site adjacent to the NNRTI pocket is a functional and biologically relevant inhibitory site. The binding of MK3 was sufficient to outcompete and displace the cocrystallized NNRTI, nevirapine. The alternate binding site of MK3 is similar to the binding site for DHBNH, which was also found to inhibit RNase H activity (Fig. 6) and was not found to bind to the RNase H active site (16). However, the inability of DHBNH to bind to the active site could be due to the occlusion of the active site by a neighboring molecule in the crystal packing in the monoclinic, C2 crystal form used. Al-

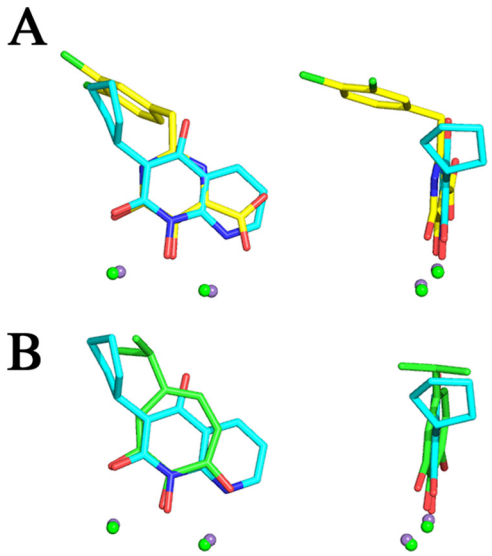

FIG. 7. Comparison between the binding of naphthyridinones with other RNase H binding inhibitors. (A) Overlay of MK2 (cyan) with the pyrimidal carboxylic acid inhibitor (yellow) (PDB code: 3HYF) (18). On the right is a rotated view showing the overlap of the planes of the metal-coordinating scaffold. (B) Overlay of MK2 (cyan) with betathujaplicinol (green) (PDB code: 3IG1) (15) and a rotated view illustrating the overlap of the metal-coordinating scaffold. The Mn^{2+} ions from the MK2 structure are shown in green; the Mn^{2+} ions from the other compared structures are shown in gray.

though DHBNH was cocrystallized with RT, the kinetics of crystal packing could have selected for molecules of RT that did not have inhibitor bound to the RNase H active site. Himmel et al. suggest the possibility of a second binding site for DHBNH from kinetic data showing that DHBNH inhibits equally well in the presence or absence of the NNRTI nevirapine (16). It is also supported by Kovacic, who describes metal chelation sites within DHBNH, although metals are not bound to the inhibitor in the crystal structure (20). The alternate, nonactive site, binding pocket may be worth further exploration. As described by Himmel et al., the binding pocket is made of a number of hydrophobic interactions which are similar to those seen in the MK3 structure. Although MK3 did not show increased potency over MK1 and MK2, it may still be possible to design inhibitors based on the structures of MK3 and DHBNH. The pocket's proximity to the NNRTI pocket may be useful for the structure-based design of new NNRTIs.

During the preparation of this report, two structures of inhibitors bound to the HIV RNase H active were published (15, 18). Despite the differences between the pyrimidal carboxylic acid scaffold that was described by Kirshberg et al., the betathujaplicinol described by Himmel et al., and the naphthyridinones described herein, all of the inhibitors appear to use two metal ions to coordinate the inhibitor with the active site residues. This suggests that coordinating both ions may aid the development of potent inhibitors. It should be noted that all published structures have been determined with Mn^{2+} as a surrogate for Mg^{2+}. In Fig. 7, the two inhibitors are shown in overlay with MK2, structurally aligned based on the RNase H domains; the metal ions overlap in the structures, suggesting that similar coordination of both ions may aid the development of potent inhibitors. The planes of the metal-coordinating pharmacophores also overlay well, in contrast with the binding of the MK3 napthyridinone (Fig. 5C). Additional published structures may reveal the impact of maintaining this plane of binding to affinity. It is also noteworthy that groups extending off the metal-binding pharmacophores are oriented in the same direction, toward HIS539, and have interactions similar to those of the cyclopentyl group of MK2.

Small molecule inhibitors against HIV have been available for close to two decades. The high mutation rate of HIV has made it difficult to combat HIV, but targeting multiple enzymes simultaneously has been effectively utilized for combination, drug treatment therapy. RNase H proteins are native to all forms of life, so building inhibitor specificity toward HIV RNase H could be critical to developing an effective drug. Structure may help the design of inhibitors that are specific to HIV and do not inhibit critical cellular enzymes. Identifying inhibitors that target new, distinct HIV activities will increase the repertoire of drugs to fight this devastating disease.

ACKNOWLEDGMENTS

We thank Suzanne Edavettal and Joan Zugay-Murphy for help with project-related protein purification outside the scope of the manuscript. We also thank Brad Feuston for insightful discussions.

Use of the IMCA-CAT beamline 17-BM at the Advanced Photon Source was supported by the companies of the Industrial Macromolecular Crystallography Association through a contract with the Center for Advanced Radiation Sources at the University of Chicago.

REFERENCES

1. **Borkow, G., R. S. Fletcher, J. Barnard, D. Arion, D. Motakis, G. I. Dmitrienko, and M. A. Parniak.** 1997. Inhibition of the ribonuclease H and DNA polymerase activities of HIV-1 reverse transcriptase by N-(4-tert-butylbenzoyl)-2-hydroxy-1-naphthaldehyde hydrazone. Biochemistry **36:**3179–3185.
2. **Cerritelli, S. M., and R. J. Crouch.** 2009. Ribonuclease H: the enzymes in eukaryotes. FEBS J. **276:**1494–1505.
3. **Cerritelli, S. M., E. G. Frolova, C. Feng, A. Grinberg, P. E. Love, and R. J. Crouch.** 2003. Failure to produce mitochondrial DNA results in embryonic lethality in *Rnaseh1*-null mice. Mol. Cell **11:**807–815.
4. **Cristofaro, J. V., J. W. Rausch, S. F. Le Grice, and J. J. DeStefano.** 2002. Mutations in the ribonuclease H active site of HIV-RT reveal a role for this site in stabilizing enzyme-primer-template binding. Biochemistry **41:**10968–10975.
5. **Crow, Y. J., A. Leitch, B. E. Hayward, A. Garner, R. Parmar, E. Griffith, M. Ali, C. Semple, J. Aicardi, R. Babul-Hirji, C. Baumann, P. Baxter, E. Bertini, K. E. Chandler, D. Chitayat, D. Cau, C. Dery, E. Fazzi, C. Goizet, M. D. King, J. Klepper, D. Lacombe, G. Lanzi, H. Lyall, M. L. Martinez-Frias, M. Mathieu, C. McKeown, A. Monier, Y. Oade, O. W. Quarrell, C. D. Rittey, R. C. Rogers, A. Sanchis, J. B. Stephenson, U. Tacke, M. Till, J. L. Tolmie, P. Tomlin, T. Voit, B. Weschke, C. G. Woods, P. Lebon, D. T. Bonthron, C. P. Ponting, and A. P. Jackson.** 2006. Mutations in genes encoding ribonuclease H2 subunits cause Aicardi-Goutieres syndrome and mimic congenital viral brain infection. Nat. Genet. **38:**910–916.
6. **Cummings, M. D., M. A. Farnum, and M. I. Nelen.** 2006. Universal screening methods and applications of ThermoFluor. J. Biomol. Screen. **11:**854–863.
7. **Davies, J. F., II, Z. Hostomska, Z. Hostomsky, S. R. Jordan, and D. A. Matthews.** 1991. Crystal structure of the ribonuclease H domain of HIV-1 reverse transcriptase. Science **252:**88–95.
8. **DeLano, W. L.** 2002. The PyMOL molecular graphics system. DeLano Scientific, San Carlos, CA. http://www.pymol.org.
9. **DHHS.** 2008. HIV and its treatment: what you should know. U.S. Department of Health and Human Services, Washington, DC.
10. **Emsley, P., and K. Cowtan.** 2004. Coot: model-building tools for molecular graphics. Acta Crystallogr. D Biol. Crystallogr. **60:**2126–2132.
11. **Fields, B. N., D. M. Knipe, and P. M. Howley.** 1996. Fields virology, 3rd ed. Lippincott-Raven Publishers, Philadelphia, PA.
12. **Hansen, J., T. Schulze, W. Mellert, and K. Moelling.** 1988. Identification and characterization of HIV-specific RNase H by monoclonal antibody. EMBO J. **7:**239–243.
13. **Hansen, J., T. Schulze, and K. Moelling.** 1987. RNase H activity associated with bacterially expressed reverse transcriptase of human T-cell lymphotropic virus III/lymphadenopathy-associated virus. J. Biol. Chem. **262:**12393–12396.

14. **Hazuda, D. J., N. J. Anthony, R. P. Gomez, S. M. Jolly, J. S. Wai, L. Zhuang, T. E. Fisher, M. Embrey, J. P. Guare, Jr., M. S. Egbertson, J. P. Vacca, J. R. Huff, P. J. Felock, M. V. Witmer, K. A. Stillmock, R. Danovich, J. Grobler, M. D. Miller, A. S. Espeseth, L. Jin, I. W. Chen, J. H. Lin, K. Kassahun, J. D. Ellis, B. K. Wong, W. Xu, P. G. Pearson, W. A. Schleif, R. Cortese, E. Emini, V. Summa, M. K. Holloway, and S. D. Young.** 2004. A naphthyridine carboxamide provides evidence for discordant resistance between mechanistically identical inhibitors of HIV-1 integrase. Proc. Natl. Acad. Sci. U. S. A. **101:**11233–11238.
15. **Himmel, D. M., K. A. Maegley, T. A. Pauly, J. D. Bauman, K. Das, C. Dharia, A. D. Clark, Jr., K. Ryan, M. J. Hickey, R. A. Love, S. H. Hughes, S. Bergqvist, and E. Arnold.** 2009. Structure of HIV-1 reverse transcriptase with the inhibitor beta-Thujaplicinol bound at the RNase H active site. Structure **17:**1625–1635.
16. **Himmel, D. M., S. G. Sarafianos, S. Dharmasena, M. M. Hossain, K. McCoy-Simandle, T. Ilina, A. D. Clark, Jr., J. L. Knight, J. G. Julias, P. K. Clark, K. Krogh-Jespersen, R. M. Levy, S. H. Hughes, M. A. Parniak, and E. Arnold.** 2006. HIV-1 reverse transcriptase structure with RNase H inhibitor dihydroxy benzoyl naphthyl hydrazone bound at a novel site. ACS Chem. Biol. **1:**702–712.
17. **Julias, J. G., M. J. McWilliams, S. G. Sarafianos, E. Arnold, and S. H. Hughes.** 2002. Mutations in the RNase H domain of HIV-1 reverse transcriptase affect the initiation of DNA synthesis and the specificity of RNase H cleavage in vivo. Proc. Natl. Acad. Sci. U. S. A. **99:**9515–9520.
18. **Kirschberg, T. A., M. Balakrishnan, N. H. Squires, T. Barnes, K. M. Brendza, X. Chen, E. J. Eisenberg, W. Jin, N. Kutty, S. Leavitt, A. Liclican, Q. Liu, X. Liu, J. Mak, J. K. Perry, M. Wang, W. J. Watkins, and E. B. Lansdon.** 2009. RNase H active site inhibitors of human immunodeficiency virus type 1 reverse transcriptase: design, biochemical activity, and structural information. J. Med. Chem. **52:**5781–5784.
19. **Kohlstaedt, L. A., J. Wang, J. M. Friedman, P. A. Rice, and T. A. Steitz.** 1992. Crystal structure at 3.5 Å resolution of HIV-1 reverse transcriptase complexed with an inhibitor. Science **256:**1783–1790.
20. **Kovacic, P.** 2008. Does structural commonality of metal complex formation by PAC-1 (anticancer), DHBNH (anti-HIV), AHL (autoinducer), and UCS1025A (anticancer) denote mechanistic similarity? Signal transduction and medical aspects. J. Recept. Signal Transduct. Res. **28:**141–152.
21. **Laskowski, R. A., D. S. Moss, and J. M. Thornton.** 1993. PROCHECK: a program to check the stereochemical quality of protein structures. J. Appl. Crystallogr. **26:**283–291.
22. **Lindberg, J., S. Sigurdsson, S. Lowgren, H. O. Andersson, C. Sahlberg, R. Noreen, K. Fridborg, H. Zhang, and T. Unge.** 2002. Structural basis for the inhibitory efficacy of efavirenz (DMP-266), MSC194 and PNU142721 toward the HIV-1 RT K103N mutant. Eur. J. Biochem. **269:**1670–1677.
23. **Martin, J. L., J. E. Wilson, R. L. Haynes, and P. A. Furman.** 1993. Mechanism of resistance of human immunodeficiency virus type 1 to 2′,3′-dideoxyinosine. Proc. Natl. Acad. Sci. U. S. A. **90:**6135–6139.
24. **Merluzzi, V. J., K. D. Hargrave, M. Labadia, K. Grozinger, M. Skoog, J. C. Wu, C. K. Shih, K. Eckner, S. Hattox, J. Adams, et al.** 1990. Inhibition of HIV-1 replication by a nonnucleoside reverse transcriptase inhibitor. Science **250:**1411–1413.
25. **Mizrahi, V., R. L. Brooksbank, and N. C. Nkabinde.** 1994. Mutagenesis of the conserved aspartic acid 443, glutamic acid 478, asparagine 494, and aspartic acid 498 residues in the ribonuclease H domain of p66/p51 human immunodeficiency virus type I reverse transcriptase: expression and biochemical analysis. J. Biol. Chem. **269:**19245–19249.
26. **Murshudov, G. N., A. A. Vagin, and E. J. Dodson.** 1997. Refinement of macromolecular structures by the maximum-likelihood method. Acta Crystallogr. D Biol. Crystallogr. **53:**240–255.
27. **Nowotny, M., S. A. Gaidamakov, R. J. Crouch, and W. Yang.** 2005. Crystal structures of RNase H bound to an RNA/DNA hybrid: substrate specificity and metal-dependent catalysis. Cell **121:**1005–1016.
28. **Nowotny, M., S. A. Gaidamakov, R. Ghirlando, S. M. Cerritelli, R. J. Crouch, and W. Yang.** 2007. Structure of human RNase H1 complexed with an RNA/DNA hybrid: insight into HIV reverse transcription. Mol. Cell **28:**264–276.
29. **Nowotny, M., and W. Yang.** 2006. Stepwise analyses of metal ions in RNase H catalysis from substrate destabilization to product release. EMBO J. **25:**1924–1933.
30. **Otwinowski, Z., and W. Minor.** 1997. Processing of X-ray diffraction data collected in oscillation mode. Methods Enzymol. **276:**307–326.
31. **Pantoliano, M. W., E. C. Petrella, J. D. Kwasnoski, V. S. Lobanov, J. Myslik, E. Graf, T. Carver, E. Asel, B. A. Springer, P. Lane, and F. R. Salemme.** 2001. High-density miniaturized thermal shift assays as a general strategy for drug discovery. J. Biomol. Screen. **6:**429–440.
32. **Pari, K., G. A. Mueller, E. F. DeRose, T. W. Kirby, and R. E. London.** 2003. Solution structure of the RNase H domain of the HIV-1 reverse transcriptase in the presence of magnesium. Biochemistry **42:**639–650.
33. **Read, R.** 1986. Improved Fourier coefficients for maps using phases from partial structures with errors. Acta Crystallogr. Sect. A **42:**140–149.
34. **Sarafianos, S. G., B. Marchand, K. Das, D. M. Himmel, M. A. Parniak, S. H. Hughes, and E. Arnold.** 2009. Structure and function of HIV-1 reverse transcriptase: molecular mechanisms of polymerization and inhibition. J. Mol. Biol. **385:**693–713.
35. **Sluis-Cremer, N., D. Arion, and M. A. Parniak.** 2002. Destabilization of the HIV-1 reverse transcriptase dimer upon interaction with N-acyl hydrazone inhibitors. Mol. Pharmacol. **62:**398–405.
36. **UNAIDS.** 2007. AIDS epidemic update. Joint United Nations Programme on HIV/AIDS and World Health Organization, New York, NY.
37. **Yang, W., J. Y. Lee, and M. Nowotny.** 2006. Making and breaking nucleic acids: two-Mg^{2+}-ion catalysis and substrate specificity. Mol. Cell **22:**5–13.
38. **Yang, W., and T. A. Steitz.** 1995. Recombining the structures of HIV integrase, RuvC and RNase H. Structure **3:**131–134.
39. **Zhao, Z., S. E. Wolkenberg, M. Lu, V. Munshi, G. Moyer, M. Feng, A. V. Carella, L. T. Ecto, L. J. Gabryelski, M. T. Lai, S. G. Prasad, Y. Yan, G. B. McGaughey, M. D. Miller, C. W. Lindsley, G. D. Hartman, J. P. Vacca, and T. M. Williams.** 2008. Novel indole-3-sulfonamides as potent HIV nonnucleoside reverse transcriptase inhibitors (NNRTIs). Bioorg. Med. Chem. Lett. **18:**554–559.